12-14-2021

A Mathematical Model for Co-Evolution of Pandemic and Infodemic with Vaccine

Anthony Morciglio

A Mathematical Model for Co-Evolution of Pandemic and Infodemic with Vaccine

by

Anthony J Morciglio

Under the Direction of Yi Jiang, PhD

A Thesis Submitted in Partial Fulfillment of the Requirements for the Degree of

Master of Science

in the College of Arts and Sciences

Georgia State University

2021

ABSTRACT

Vaccine hesitancy, resulting from bad information, threatens the possibility of ending the COVID-19 pandemic through mass vaccination. The COVID-19 pandemic coincides with an overabundance of controversial information regarding disease transmission and public health mitigation approaches. We investigate a phenomenological co-evolution of pandemic and infodemic in the context of COVID-19 with an emphasis on evolutionary game theory. Using bifurcation analysis, we determine the limit cycle boundaries and the separation of attraction between stable foci of infection and periodic outbreaks of infection. Our results suggest that low risk perception of vaccination relative to infection is not sufficient to eradicate the disease; promotion of quarantine methods or targeted mitigation of the spread of corona-misinformation is necessary to drive the system to disease free equilibrium.

INDEX WORDS: Infodemic, Pandemic, Vaccination, COVID-19, Model, Co-Evolution, Game Theory

A Co-Evolution of Pandemic and Infodemic

by

Anthony J Morciglio

Committee Chair: Yi Jiang

Committee: Alexandra Smirnova

Igor Belykh

Electronic Version Approved:

Office of Graduate Services

College of Arts and Sciences

Georgia State University

December 2021

DEDICATION

This thesis is dedicated to the memory of innocent souls lost and acknowledgement of irreparable damages from the COVID-19 pandemic. I honor their interrupted lives, unrealized potentials, and undiscovered purposes taken from our world. I also honor the selfless love and unrelenting dedication from front-line workers that risk physical and mental health each day to care for those in our society struggling with this virus and its lingering effects. I dedicate my work for their testament of perseverance in the face of unabating challenge to cope and live in our world crippled and forever changed in many ways by this virus.

Anthony honor's all his family, friends, and colleagues supporting him in this long and enduring journey. I appreciate all those that have helped and guided me to the journey of achieving my degree.

ACKNOWLEDGEMENTS

Anthony would like to thank his advisors for their guidance and sponsorship. It was a significant help in this complex process of organization, discovery, and encouragement with the pressures of obtaining a master's degree in mathematics. I would like to thank his PI, Yi, for her patience and ability to teach me to see that research focuses on the bigger picture. Anthony would like to thank Alexandria for her teaching and team competition in Vector Calculus and Optimization courses. Anthony would like to thank Igor for his teaching in the Advanced Mathematical Biology course. Anthony would like to thank the faculty and staff at the prestigious Georgia State University for their continued support and leadership.

This work was partially supported a 2CI PhD Fellowship from Georgia State University (to AM). Thank those who helped you through this research. Anthony would like to thank his advisor: Dr. Yi Jiang, Georgia State University, all previous instructors in his undergraduate and graduate program, and colleagues at the lab.

Lastly, I would like to thank my high school instructors: Dr. Vermilya, Mrs. Lucking, and Mr. Grummer. If it were not for their interest in my future education and determination to convince me to explore my interests and ask questions, I would not have obtained a degree in Mathematics. Nor would I have transitioned from the suburban community of Woodstock, GA to the large urban city in Atlanta, Georgia, and never would I have thought of pursuing a master's degree in Mathematics with the dream of learning Mathematics. I thank them, my parents, and close relatives for building confidence in my abilities, challenging my foundation, and pushing me to my intellectual limits.

TABLE OF CONTENTS

LIST OF TABLES

LIST OF FIGURES

LIST OF ABBREVIATIONS

BP: Branching Point Bifurcation

BT: Bogdanov-Takens

CDC: Center for Disease Control

CP: Cusp

DFE: Disease Free Equilibrium

DH: Double Hopf Bifurcation

GH: Generalized Hopf Bifurcation

H: Andronov Hopf Bifurcation

LP: Limit Point

LSA: Local Sensitivity Analyses

NS: Neutral Saddle Equilibrium

NSr's: Neimark-Sacker

R_0: Basic Reproductive Number

Re: Effective Reproductive Number

SEIR: Susceptible-Exposed-Infectious-Recovered

SIS: Susceptible-Infectious-Susceptible

UK: United Kingdom

UN: United Nations

WHO: World Health Organization

1 INTRODUCTION

The COVID-19 pandemic, caused by SARS-CoV-2, presents an unprecedented challenge to human health, the economy, and nearly all aspects of our society. COVID-19 vaccination and practicing of CDC guidelines is the only sustainable mitigation to prevent widespread morbidity and mortality from the infection. Vaccine hesitancy, a strong unwillingness to adopt the vaccination independent of morbidity and perceived risk [24, 29], remains a barrier to the achievement of herd immunity. It is difficult to comprehend that some of the greatest triumphs of medical science are being eroded by the promotion corona-misinformation and corona-distrust [26]. In February 2020, the World Health Organization (WHO) started using the term infodemic for the overabundance and spread of good and bad information about disease transmission and public health mitigation approaches. The spread of corona-misinformation makes it difficult for people to ascertain trustworthy sources and reliable guidance when they need it [37]. The WHO, the United Nations (UN) UNICEF, and other major world health organizations issued a joint statement in September 2020 calling for member states to "manage the COVID-19 infodemic, to promote healthy behaviors and mitigate the harm from corona-misinformation and corona-disinformation [40]. To address vaccine hesitancy and the role of infodemic in driving the COVID-19 pandemic, we consider a novel model to understanding the dynamics of the co-evolution of epidemics and infodemics with vaccination considered. An infodemic requires an overabundance of information, communication between news outlets and readers and spreads like an epidemic among humans through digital and physical outlets. We choose to model the spread of information like the spread of infection, using simple non-linear reaction approximations for the rate of information exchange. We incorporate an evolutionary game theoretical framework to evaluate the role of risk of infection to an extended COVID-19

infodemic model to help understand how the spread of good and bad information impact disease transmission. Vaccine hesitancy remains a barrier to population inoculation against highly infectious diseases such as SARS-CoV-2. As mass COVID-19 vaccination efforts underway around the world, significant vaccine hesitancy, and resistance observed by healthcare workers [15, 22] and ethnic minority groups continues to rise [28, 31]. Concerns about the safety of the vaccine contribute to vaccine hesitancy. Distrust in the scientific expertise and health and government authorities drives consumers away from traditional sources (newspapers, television, radio, government agencies) to social media outlets [28], who are then more likely recipients of bad information. Recent new studies have begun to classify and quantify the spread of bad information about COVID-19 [32, 33]. A study, based on a national survey of US adults in March and July of 2020, found that about 15% believed the pharmaceutical industry created the coronavirus and more than 28% thought it was a bioweapon made by the Chinese government. Those beliefs predicated a subsequent decrease in willingness to wear a mask or take a vaccine [32]. An analysis of bad information from five countries (the United States, the UK, Ireland, Spain, and Mexico showed that substantial portions of each population - anywhere from 15% to 37% - believed bad information about COVID-19 in April and May 2020, representing what the authors call a “major threat to public health.” People who are more gullible to corona-misinformation are less likely to comply with public health recommendations and less likely to become vaccinated [33]. Most studies on the spread of information focus on the contribution of social media platforms such as Facebook, Twitter, and WhatsApp act as functional conduits in the surge of bad information [2, 12, 27, 42]. These models suggest that the transmission of corona-misinformation, is a palpable risk to society; facilitating public distrust and impeding the CDC advised practices including mask wearing, social distancing, and quarantining following

infection. Preceding the COVID-19 pandemic, one study used an agent-based model of a norovirus outbreak to show that reducing bad information by 30% or making at least 30% of the population fully resistant to sharing bad information, was effective in counteracting the negative impacts of bad advice on the outbreak [7]. Another study, using a susceptible-infectious-susceptible (SIS) epidemic model on a scale free network incorporated media mitigated reduction in infection and showed that the spread of good information can impede infection by decreasing the basic reproductive number [39]. Additionally, both models considered the spread of infection as influenced by the spread of information yet lacked the feedback of infection on the spread of information. One more study used a susceptible-exposed-infectious-recovered (SEIR) model on a bipartite network (a physical social network for epidemics and a separate information spread network for social influence) coupled with risk perception of infection to information in the onset of epidemic [41]. Their results suggest that although heavy non-pharmaceutical intervention greatly reduces the epidemic spread, high socioeconomic cost associated with these interventions will prevent their implementation [41]. None of these previous network models included vaccination [7, 39, 41]. We propose a mathematical model that couples epidemiology with evolutionary game theory to help understand the co-evolution of epidemic and infodemic in the presence of vaccination. We use a stratified SIS model for viral infection, accounting for the possibility of reinfection through the emergence of different viral variants. We stratify the population to those with ’good’ and ’bad’ information. People with ’good’ information follow science-based advice, practice precautionary measures issued by CDC including following guidelines on wearing mask, keeping social distance, and becoming vaccinated when possible. People with ’bad’ information behave contrarily and propagate the spread of disease. We model the spread of information using a similar framework as models for

the spread of infections, people with ’good’ information are misinformed by the ’bad’ and change their behavior accordingly. Furthermore, we consider the probability of ’good’ becoming vaccinated, which depends upon the perception of risk of vaccination relative to infection and is derived using an evolutionary game theoretical framework. Our co-evolution model of pandemic and infodemic exhibits complex dynamics stable foci of high infection at high rates of bad information spread (Figures: 2.6.1, 2.6.2, 2.6.3), stable periodic oscillations of infection at low rates of good information spread (Figures: 2.9.1, 2.9.2), and mixed oscillations at high values of risk perception (Figure 2.7.1). We find that the spread of bad information feeds the infectious disease spread, allowing periodic outbreaks even for 90% vaccination efficacy in reducing the infection. Although reducing the perception of risk of vaccination increases the vaccination uptake, promotion of good information or reduction of bad information drives the system to disease free state. Our results suggest that increasing the trust of the public, e.g., reducing the risk perception of the vaccination, is not sufficient in the achievement of herd immunity; additional mitigation methods that focus on the spread of information are needed to promote the health of the population.

1.1 Background

Previous models have considered the reduction of infection that depends on media coverage [39], the mitigation of disease in contrast to socioeconomic cost [41], and the incorporation of relative vaccination morbidity relative to infection mortality [7]. One model considered a degree distribution of infection and performed static analysis on the basic reproductive number. Suppose there are $S = \{N_1, N_2, \ldots, N_n\}$ distinct nodes of degree N_j. The degree distribution, P_j, can be expressed as the relative fraction of each degree node divided by the cumulative sum:

$$\frac{N_j}{N_1 + N_2 + \cdots + N_n} \tag{1.1}$$

The first moment of the degree distribution, or commonly referred to as the mean degree, is expressed as:

$$\langle k \rangle = k_j P_j \tag{1.2}$$

In the classical SIS model, one considers the following set of two equations:

$$\frac{dS}{dt} = -\beta^* SI + \mu I \tag{1.3}$$

$$\frac{dI}{dt} = \beta^* SI - \mu I \tag{1.4}$$

Where β* is the effective transmissibility of infection and μ is the disease recovery rate. In a heterogeneous model, the probability of running into the susceptible depends on the degree distribution, the density function, Θ, which is proportional to the fraction of infected with degree k, I_k:

$$\Theta = \frac{\sum(kP_k)}{\langle k \rangle} \frac{I_k}{N_k} \tag{1.5}$$

Where <k> is the mean degree (1.2), $N_k = S_k + I_k$, and P_k is the degree distribution (1.1). Substitution of density function (1.5) into equations (1.1, 1.2), gives the following:

$$\frac{dS}{dt} = -\beta\Theta\, S_k + \mu I_k \tag{1.6}$$

$$\frac{dI}{dt} = \beta\Theta\, S_k - \mu I_k \tag{1.7}$$

Yi Wang considers the infectious dynamics of binge drinking: taking S_k as the susceptible fraction with no or moderate drinking habits, X_k as the aware fraction that avoids encountering the binge drinking fraction of population I_k. Substituting the effective probability of infection, β* = βΘ, one has the following:

$$\frac{dS_k}{dt} = -\beta\Theta S_k + \mu I_k - \alpha S_k M - \sigma X_k \quad (1.8)$$

$$\frac{dX_k}{dt} = \alpha S_k M - \sigma X_k \quad (1.9)$$

$$\frac{dI_k}{dt} = \beta S_k \Theta - \mu I_k \quad (1.10)$$

$$\frac{dM}{dt} = \omega\Sigma(I_k) - \gamma M \quad (1.11)$$

Where M is the media of awareness of infection and serves as the good information that reduces the severity of the epidemic, μ is the recovery rate of the binge drinkers, α is the dissemination rate of awareness among non/moderate drinkers, ω is the growth rate of media coverage, γ is the depletion of media coverage due to ineffective measures, and σ is the transmission rate from aware individuals to non/moderate drinkers [37]. In this manuscript, we consider the good information to promote quarantine methods following infection.

Another model considers a bipartite network G = (V, E_i, $E_c(t)$) that incorporates information exchange and disease spread concomitantly where V = {V_1, V_2, …, V_n} is the collection of n individuals and E_i and $E_c(t)$ correspond to the influence and contact layer respectively. In Ye's analysis, the influence layer is static and does not evolve in time. In the disease domain, each element, i, takes on a health status of healthy at x_i or infected at y_i. Taking A_k = {S_k, I_k} to consist of all individuals of with degree k, Ye chooses to model the infectious dynamics using an SIR approach. Let R = N – S - I be the removed fraction of the population Under the assumption of no vital dynamics, the transmission of infection can be described as:

$$\frac{dS_k}{dt} = -\lambda\Theta S_k \quad (1.12)$$

$$\frac{dI_k}{dt} = \lambda\Theta S_k - \mu I_k \quad (1.13)$$

$$\frac{dR}{dt} = \mu \Sigma I_k \tag{1.14}$$

Ye takes a unique modelling approach and considers non-linear modelling of policy decision making, risk perception function, and associated cost of self-protective behavior. Their paper considers the payoff function to depend on policy decision and risk perception and is formulated using network coordination type games [41]. In this manuscript, we consider the homogeneous model that focuses on the risk payoff which does not depend on policy decision nor degree distribution, but on the relative risk of vaccination to infection (Section 2.3, [7]).

2 RESULTS

2.1 A Mathematical Model for the Coevolution of Epidemic and Infodemic

We consider a stratified SIS model for both virus and information spread to model the co-evolution of epidemic and infodemic. In the disease domain, the population is divided into susceptible (S), infectious (I), and vaccinated (V). In the information domain, the population consists of two mutually exclusive compartments: those with good information practice behavior restrictive public health measures to reduce spread of disease; including mask wearing, social distancing, and a likelihood of receiving vaccination. Likewise, those with bad information contribute to the spread of infection and bad information. We model the spread of information analogous to an infectious process requiring physical contact between good and bad fractions in the information domain. Additionally, we make a strong assumption that those infected with good information (I_G) follow CDC guidelines and practice self-quarantine. Therefore, only the infected people with bad information (I_B) transmit the virus and drive the epidemic spread. Throughout this manuscript, we evaluate the phenomenological role of perception of risk of vaccination, rates of spread of good and bad information that drive the complex dynamics between pandemic and infodemic. We find that decreasing the perception of risk of vaccination, promoting the spread of good information, and reducing the spread of bad information promotes the achievement of herd immunity. As illustrated in the schematic diagram (Figure 2.1.1), a susceptible person with good information (S_G) is exposed to the force of infection by I_B to become infected with good behavior (I_G) or are recipients of bad information and become (S_B). A bad behaving infected person (I_B) can recover from the disease and become a susceptible person with bad behaviors S_B at rate γ or be 'educated' at rate ϵ to become I_G. We assume that the transmission of good information of those infected with bad information is proportional to the

contact to good information. The susceptible with good information S_G become vaccinated with probability φ. Vaccinated people are temporarily immune with efficacy δ. The vaccination compartment serves as a vaccination leakage for $\delta < 1$.

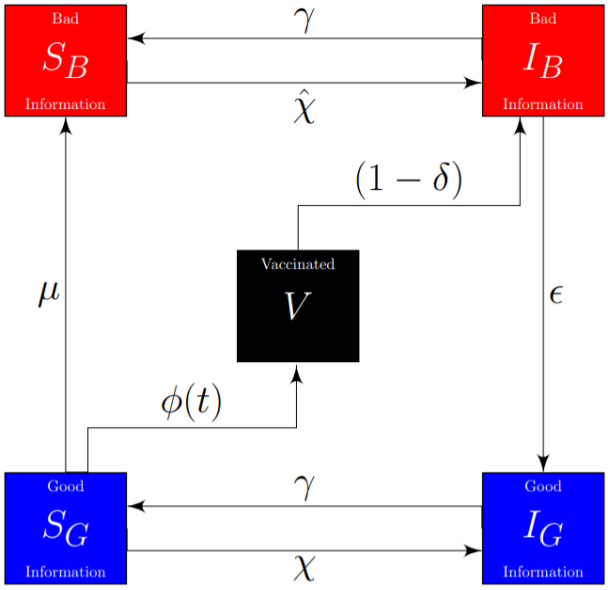

Figure 2.1.1 Schematic representation of co-evolution of infodemic and pandemic. The susceptible population with good information, S_G, is infected with corona-misinformation and virus at transmission probabilities: μ and χ respectively. The susceptible with bad information S_B have an increased force of infection $\chi < \hat{\chi}$. Once a susceptible becomes infected, they recover at rate γ. Additionally, the misinformed infectious I_B become educated at rate ϵ. The probability that a susceptible person with good information, S_G, becomes vaccinated with probability φ. The vaccination compartment acts as a leakage and become re-infected.

In the absence of vital dynamics, conservation implies: $S_G + S_B + I_G + I_B + V = 1$. Throughout this manuscript, we use the following composite quantities: Bad ($B = I_B + S_B$), Good ($G = I_G + S_G$), Infected ($I = I_G + I_B$), and Healthy ($H = S_G + S_B + V$). In the disease domain (the horizontal directions of Figure 2.1.1), we assume that both infected populations: I_G and I_B, recover at rate γ, but bad-behaving susceptible, S_B, are infected at a higher rate than that for good-behaving susceptible ($\chi < \hat{\chi}$). In the information domain (the vertical direction of Figure 2.1.1), we assume S_G is misinformed by those with the bad information, B, at transmission probability μ; those

infected with bad information, I_B, are educated through exposure to those with good information, G, at transmission probability ϵ. We further assume that the probability of vaccination uptake depends on the relative perception risk of vaccination relative to infection, r. We use game theoretical framework to model the human decision-making on vaccination [6]. In a traditional vaccination game, the payoff of an individual taking a vaccine is greater when the morbidity risk is lower. In the context of COVID-19, the vaccination hesitancy is not due to vaccination morbidity but may depend on risk perception of vaccination relative to infection [28, 31]. We use r_v and r_i to denote the perceived risks of vaccination and infection, respectively, and define the relative risk perception as $r = r_v/r_i$. The probability of vaccination φ depends on the strength of initiative parameter, m, and payoff gained for adopting the vaccination strategy compared with individuals who do not take the vaccination [6, 21]. The strength of initiative is a proportionality constant that determines the speed of convergence at which those with the susceptible population with the good information become vaccinated, which we assume to be constant (Section 2.3). The co-evolution of pandemic and infodemic with the incorporation of vaccination are described as:

$$\frac{dS_G}{dt} = \gamma I_G - \phi S_G - \chi S_G I_B - \mu S_G(I_B + S_B) \quad (2.1.1)$$

$$\frac{dS_B}{dt} = \gamma I_B + \mu S_G(S_B + I_B) - \hat{\chi} S_B I_B \quad (2.1.2)$$

$$\frac{dI_G}{dt} = -\gamma I_G + \epsilon(S_G + I_G) I_B + \chi S_G I_B \quad (2.1.3)$$

$$\frac{dI_B}{dt} = -\gamma I_B + \hat{\chi} S_B I_B - \epsilon(S_G + I_G) I_B + (1-\delta)\chi V I_B \quad (2.1.4)$$

$$\frac{dV}{dt} = \phi S_G - (1-\delta)\chi V I_B \quad (2.1.5)$$

$$\frac{d\phi}{dt} = m\phi(1-\phi)(I_G + I_B - rV) \quad (2.1.6)$$

In these equations, the transmission rates of "bad" information spread, and "good" information spread are μ and ϵ, respectively, which we refer to as corona-misinformation and education. Although information spreads faster than virus transmission in the digital landscape [41], the rate for a person to change their opinion upon receiving information varies greatly. Hence, in our mean-field model, without the separation of information and physical networks, the rate of information transmission (for μ and ϵ) can be greater or less than those for viral infection. Without loss of generality, we assume the spread of corona-misinformation is less than infection ($\mu < \hat{\chi}$), and the rate for education exceeds the intrinsic disease recovery rate ($\epsilon > \gamma$) (Table 2.1.1).

Table 2.1.1 Model parameters and their baseline values. All parameters are unitless, except for γ with unit 1/ day. Note that: γ, χ, χˆand m are kept constant in the simulations reported below.

Parameter	Description	Value
ϵ	Transmission probability of good information on I_B	0.33
μ	Transmission probability of bad information on S_G	0.10
$\hat{\chi}$	Transmission probability of virus of S_B to I_B	0.37
χ	Transmission probability of virus of I_B to S_G	0.048
δ	Vaccination efficacy (protection)	0.90
γ	Disease recovery rate	0.07
r	Perception of risk of vaccination relative to infection	1.635
m	Strength of initiative	1.0

In this set of baseline parameters, we choose γ = 0.07 to reflect the 14-day incubation period, and $\hat{\chi}$ = 0.37 such that R_0 = 2.5, consistent with the epidemiology of SARS-CoV-2.

To measure the prevalence of infection, we derive the effective reproductive number using the next generation matrix technique [14, 15]. When no vaccine is available, φ = 0 = V. Solving for the non-trivial fixed point in equation (2.1.4) leads to:

$$\hat{\chi}S_B - \gamma - \epsilon G = \left(\frac{\hat{\chi}S_B}{\gamma + \epsilon G} - 1\right) = 0 \tag{2.1.7}$$

where $G = S_G + I_G$ is the fraction of the population with good information. For $I_B \neq 0$, $I_G = I_B (\hat{\chi}S_B + \epsilon G) / \gamma$. Adding equations (2.1.3) and (2.1.4) together, we have:

$$I_B\left(\frac{\hat{\chi}S_B}{\gamma + \epsilon G} - 1\right) = I_B(R_0 - 1) = 0 \tag{2.1.8}$$

Thus, the effective reproductive number only depends on the infection force generated with the bad information I_B. With non-trivial probability of vaccination uptake, $\varphi \in (0, 1)$, we have:

$$I_B\left(\frac{\hat{\chi}S_B + (1-\delta)\chi V}{\gamma + \epsilon G} - 1\right) \tag{2.1.9}$$

When the term within the parenthesis in equation (2.1.9) is negative for all time $t \geq 0$, I_B will converge to 0 and the system reaches a disease-free equilibrium (DFE). Thus, we have the effective reproductive number:

$$R_e = \frac{\hat{\chi}S_B + (1-\delta)\chi V}{\gamma + \epsilon G} \tag{2.1.10}$$

Note that when V = 0 or δ = 1, Re reduces to R_0 in equation (2.1.8). We observe that the effective reproductive number inversely depends on the recovery rate: γ and the spread of good information: ϵG. Re decreases with increasing vaccination efficacy: δ and increases with probability of disease transmissibility between the bad at rate: $\hat{\chi}$. We note that the appearance of the V term in the numerator of the effective reproductive number, Re, is a consequence of the assumption of vaccination leakage where the vaccinated are re-infected by those with the bad information. Unique to our model, the inclusion of high infection on S_B by I_B at transmission

probability $\hat{\chi}$ is two orders of magnitude higher than the infection generated on V by I_B at rate $(1 - \delta)\,\chi$. For appropriate choices of the parameters, we obtain mixed oscillations and is reflected in the separation of time scales in the numerator of R_e (Figure 2.5.1).

2.2 Model Formulation

2.2.1 Model

We consider a stratified SIS framework partitioned into binary: good (S_G, I_G) vs. bad (S_B, I_B) respectively. Furthermore, we assume that the susceptible individuals with good information, S_G, take the vaccine, V, which depends on the risk function φ.

$$\frac{dS_G}{dt} = \gamma I_G - \left(\widetilde{\lambda_b} + \lambda_b + \phi\right)S_G \tag{2.2.1}$$

$$\frac{dS_B}{dt} = \gamma I_B + \widetilde{\lambda_b} S_G - \lambda_g S_B \tag{2.2.2}$$

$$\frac{dI_G}{dt} = -\gamma I_G + \alpha_g I_B + \widetilde{v_b} G \tag{2.2.3}$$

$$\frac{dI_B}{dt} = -\gamma I_G + \hat{\alpha}_b I_B - \widetilde{v_b} G + (1 - \delta)\alpha_v I_B \tag{2.2.4}$$

$$\frac{dV}{dt} = \phi S_G - (1 - \delta)\alpha_v I_B \tag{2.2.5}$$

$$\frac{d\phi}{dt} = m\phi(1 - \phi)(I - rV) \tag{2.2.6}$$

In these equations:

$$I = I_G + I_B \tag{2.2.7}$$

$$B = S_B + I_B \tag{2.2.8}$$

$$G = S_G + I_G \tag{2.2.9}$$

$$\alpha_g = c_{bg}\beta_{bg}S_G = \chi S_G \tag{2.2.10}$$

$$\alpha_v = c_{bg}\beta_{bg}V = \chi V \tag{2.2.11}$$

$$\hat{\alpha}_b = c_{bg}\beta_{bg}S_B = \hat{\chi}S_B \quad (2.2.12)$$

$$\widetilde{v_g} = c_{bg}\widetilde{\beta_g}\, S_G = \mu S_G \quad (2.2.13)$$

$$\widetilde{v_b} = c_g\widetilde{\beta_g} I_B = \epsilon I_B \quad (2.2.14)$$

2.2.2 Nullclines

Consider the state variable vector, $x = [x_1, x_2, x_3, x_4, x_5]$, and the vector function $f_j(x)$ for each $j = 1, 2, \ldots, 5$, then equations (2.1.1, 2.1.2, 2.1.4, 2.1.5, 2.1.6) can be expressed as:

$$\frac{dx_1}{dt} = f_1(x) \quad (2.2.16)$$

$$\frac{dx_2}{dt} = f_2(x) \quad (2.2.17)$$

$$\frac{dx_3}{dt} = f_3(x) \quad (2.2.18)$$

$$\frac{dx_4}{dt} = f_4(x) \quad (2.2.19)$$

$$\frac{dx_5}{dt} = f_5(x) \quad (2.2.20)$$

The nullclines and phase portraits for two distinct of the state variables are obtained by setting all equations to the right-hand side of equations (2.1.1, 2.1.2, 2.1.4, 2.1.5, 2.1.6) equal to zero. Without loss of generality, let Nx_i and Nx_j represent the nullclines in x_i and x_j respectively. The xi nullcline, Nx_i, is obtained by setting dx_i / dt equal to zero and solving for x_j. The x_j nullcline, Nx_j, is obtained by setting dx_j / dt equal to zero and solving for x_i. In our model, the S_B vs. S_G nullclines are expressed as:

$$N_{S_B} = \frac{I_B(\hat{\chi}S_B - \gamma)}{\mu(S_B + I_B)} \quad (2.2.21)$$

$$N_{S_G} = \frac{\gamma I_G - S_G(\phi^* + (\chi + \mu)I_B^*)}{\mu S_G} \quad (2.2.22)$$

Substituting $\varphi * S_G^*/I_B = (1 - \delta)\,\chi V^*$, then the I_B vs. S_B nullclines are expressed as:

$$N_{I_B} = \frac{\gamma + \epsilon(S_G^* + I_G^*) - \frac{\phi^* S_G^*}{I_B}}{\hat{\chi}} \tag{2.2.23}$$

$$N_{S_B} = \frac{\mu S_G^* S_B}{\hat{\chi} S_B - \gamma - \mu S_G^*} \tag{2.2.24}$$

The V vs. I_B nullclines are expressed as:

$$N_V = \frac{\phi^* S_G^*}{(1-\delta)\chi V} \tag{2.2.25}$$

$$N_{I_B} = \frac{\gamma + \epsilon(S_G^* + I_G^*) - \hat{\chi} S_B^*}{(1-\delta)\chi} \tag{2.2.26}$$

The I_B vs. I_G nullclines are expressed as:

$$N_{I_B} = \frac{\mu S_G^*(S_B^* + I_B) + I_B[(1-\delta)\chi V^* - \epsilon S_G^*]}{\epsilon I_B} \tag{2.2.27}$$

$$N_{I_G} = \frac{\gamma I_G}{\epsilon(S_G^* + I_G + \chi S_G^*)} \tag{2.2.28}$$

Where S_G^*, S_B^*, I_B^*, V^*, φ^*, and $I_G^* = 1 - (S_G^* + S_B^* + I_B^* + V^*)$ represent the fixed points obtained numerically using PyDSTool [11].

2.2.3 Perturbation about Steady States

After obtaining the steady state values by setting equations (2.1.1 – 2.1.6) equal to zero and solving numerically for the steady state vector $x*$ using PyDSTool [11]. We obtain a perturbed time series plot for the fixed points; we apply the following algorithm to determine the perturbation about the time series data:

1. Obtain a steady state vector, $x*$, using PyDSTool [11].

2. Generate a uniformly distributed random variable: $u = [u_1, u_2, \ldots, u_5]$.

3. Loop through each component of the steady state vector: x_j^* in each $j = 1, 2, \ldots, 5$.

4. Set: $z_j = (1 + \epsilon_0 \times \sigma_j \times u_j) \times x_j^*$, where z_j is the jth component of perturbed steady state vector z, $\sigma_j = \text{sgn}(u_j - 1/2)$ takes value of 1 or −1, and ϵ_0 is the weight of the noise. Throughout the simulation $\epsilon_0 \in (0, 0.1)$.

5. Exit the loop and use $z*$ for the new initial conditions.

2.2.4 Calculation of the Jacobian

The Jacobian of the system is computed by taking the first partials of equations (2.1.1 - 2.1.6). Without loss of generality, not considering equation (2.1.3), since conservation implies: $S_G + S_B + I_G + I_B + V = 1$, gives rise to linear dependency. The (i, j)th element of the Jacobian is the partial derivative of the ith equation with respect to the jth state variable of the state vector: $x^* = [S_G^*, S_B^*, I_B^*, V^*, \varphi^*]$. One obtains:

$J_{11} = -\gamma - [\varphi* + (\chi + \mu)I_B^* + \mu S_B^*]$, $J_{12} = -\gamma - \mu S_G^*$, $J_{13} = -\gamma - (\chi + \mu)S_G^*$, $J_{14} = -\gamma$, $J_{15} = -S_G^*$, $J_{21} = \mu(S_B^* + I_B^*)$, $J_{22} = \mu S_G^* - \hat{\chi} I_B^*$, $J_{23} = \mu S_G^* + \gamma - \hat{\chi} S_B^*$, $J_{24} = 0$, $J_{25} = 0$, $J_{31} = 0$, $J_{32} = (\hat{\chi} + \epsilon)I_B^*$, $J_{33} = \hat{\chi} S_B^* + (1 - \delta)\chi V^* - \gamma + \epsilon(S_B^* + 2I_B^* + V* - 1)$, $J_{34} = [(1 - \delta)\chi + \epsilon]I_B^*$, $J_{35} = 0$ $J_{41} = \varphi*$, $J_{42} = 0$, $J_{43} = -(1 - \delta)\chi V*$, $J_{44} = -(1 - \delta)\chi I_B^*$, $J_{45} = S_G^*$, $J_{51} = -m\varphi* (1 - \varphi*)$, $J_{52} = -m\varphi* (1 - \varphi*)$, $J_{53} = 0$, $J_{54} = -\varphi* (1 - \varphi*)(1 + r)$, $J_{55} = (1 - 2\varphi*)[1 - (S_G^* + S_B^* + (1 + r)V*)]$

Where: $J_{ij} = \partial x_i / \partial x_j$ and: S_G^*, S_B^*, I_B^*, $V*$, and $\varphi*$ represent the fixed points obtained numerically using PyDSTool [11]. A close observation of the 5th column shows that the branching point bifurcation in Figure 2.7.1 is obtained for $S_G = 0$, $\varphi = 1$, $\Delta E = 0$ giving rise to an identical zero eigenvalue, which corresponds to the unstable mixed Nash Equilibrium in the coordination game (Section 2.3 and [20]).

2.3 Game Theoretical Formulation of Vaccination

2.3.1 Deriving the Risk Function

The simplest formation of a vaccination game consists of two players: The vaccinated (V) and defector (D), whom each have a finite set of choices πV and πD respectively. For simplicity, we consider the defector (D), to take a chance to become infected (I). We consider the following payoff matrix: π is 2 x 2 matrix whose (v, w)th entry is the payoff of the vth player in response to the wth player. In the vaccination game, one obtains: $\pi_{vv} = 0$, $\pi_{vi} = -r_i I$, $\pi_{iv} = -r_v V$, and $\pi_{ii} = 0$ [6]. Where r_v and r_i are the risk perception associated to vaccination and infection respectively. For simplicity, we consider payoffs with the vaccinated and infected interact with each other (leaving the diagonal entries 0). Consider x_v and x_i the frequency of strategy selection of vaccination and defection, i.e., infection, respectively. Since our game only considers the selection of two strategies, then $x_v + x_i = 1$, thus the replicator equations for each species follows as:

$$\frac{dx_i}{dt} = x_j(\pi x)_j - x'\pi x \tag{2.3.1}$$

For each j = v, i. Since $x_v + x_i = 1$, then we can simplify the coupled replicator equations into:

$$\frac{dx}{dt} = xv \times (1 - xv) \times [(\pi x)v - (\pi x)i] \tag{2.3.2}$$

Where $(\pi x)_v - (\pi x)_i = \Delta E$ is the marginal expectation difference between the strategies [20]. According to the Bishop-Canning's Theorem, one can compute the marginal expectation difference provided there exists a non-trivial Nash equilibrium. Since our payoff matrix π in equation 2.3.2 follows a coordination game where the greatest payoffs are located along the main diagonal, then we can compute the pure Nash equilibrium, which are determined by the relative

difference in the diagonal elements [18, 20, 38]. Applying the Bishop-Cannings theorem in [20, 38] to solve for the frequency of selection, observe that:

$$x = \frac{\pi_{vi}}{\pi_{vi} + \pi_{iv}} \tag{2.3.3}$$

Where π_{vi} and π_{iv} are the expected payoffs in payoff matrix π. The marginal expectation difference follows is:

$$\Delta E = xE[v] - (1 - x)E[i] = -r_v V + r_i I \tag{2.3.4}$$

Since scaling the payoff matrix in 2.1 does not change the behavior of the game [6, 18], then the marginal expectation difference can be expressed as: $\Delta E = I - r \times V = 1 + (1 + r)\, V - S_G - S_B$, where $r = r_v / r_i$ is the dimensionless relative risk perception of vaccination to infection. Thus, the replicator equation that describes the adoption of becoming vaccinated is simply:

$$\frac{dx}{dt} = x(1 - x)\Delta E \tag{2.3.5}$$

And simplifies to equation 2.1.6 when substituting $x = \varphi$ and multiplying by the strength of initiative parameter m.

2.3.2 Computing the Nash Equilibrium

Since the payoff matrix in has diagonal elements identically equal to zero, then we can compute the Nash equilibrium. Consider $\varphi_v \in (0, 1)$ the non-trivial probability of vaccination uptake. Observe that the replicator equation in equations (2.1.6, 2.3.5) exhibits the following dynamics:

Table 2.3.1 Marginal expectation difference ΔE in equation 2.1.6 with respect to risk perception of vaccination relative to infection, r, fraction of vaccinated V, and fraction of

infected I. The parameter range for the incentive to vaccinate is greater at higher levels of infection as compared to vaccination.

Risk	$V > I$	$V \leq I$
$r \leq 1$	$\exists\, r_* \in (0,\ 1):\ \Delta\mathbb{E} > 0\ \forall\ r\ \in (0,\ r_*)$ $\Delta\mathbb{E} \leq 0\ \forall\ r \in [r_*,\ 1]$	$\Delta\mathbb{E} \geq 0\ \forall\ r \in (0,\ 1]$
$r > 1$	$\Delta\mathbb{E} < 0\ \forall\ r > 1$	$\exists\, r_* \geq 1:\ \Delta\mathbb{E} \geq 0\ \forall\ r \in [1,\ r_*)$ $\Delta\mathbb{E} < 0\ \forall\ r > r_*$

For any given time, t, when the vaccinated, V, is smaller than or equal to the fraction infected, I, the sensitivity about the perception of risk has a larger range for positive incentive to vaccinate $\Delta E \geq 0$ when $r \in (0, r*)$ and $r* > 1$ (Table 2.3.1: column 2). This suggests that in the early stages of the epidemic, the perception of risk is less sensitive to increasing the fraction of the population to become infected. The value of risk, r, that drives the risk function to an unstable equilibrium in equation 2.1.6 corresponds to the emergence of stable oscillations in the branching point bifurcation (Figure 2.7.1). The oscillations in φ are also a reflection of the mixed unstable Nash equilibrium in the coordination game [20]. During the later stages of the pandemic, the fraction of infected begin to decrease as the population begins to take the vaccine. For any given time, t, when the vaccinated exceeds the cumulative infected and the incentive to vaccinate only exists for $r \in (0, r*)$ where $r* < 1$ (Table 2.3.1: column 3). The value of $r*$ that corresponds to the incentive to vaccinate identically equal to zero, $\Delta E = 0$, corresponding to the emergence of limit cycles along the branching point bifurcation (Figures: 2.6.1, 2.7.1).

2.4 Local Sensitivity Analyses

We perform local sensitivity analysis (LSA) about the baseline parameters in Table 2.1.1. The goal of local sensitivity analysis is to evaluate the outputs of the model (QOI's) with respect to key parameters of interest (POI's). The most sensitive parameters have the most potent effects with respect to small deviations from an initial value [4]. If $\hat{p}$ and $\hat{q}$ are estimated parameter and

quantities of interest respectively, and $\hat{q}$ = Q ($\hat{p}$). Then, we can perturb the parameter of interest slightly to evaluate the local sensitivity. One defines the sensitivity indices:

$$S(p,q) = \frac{p}{q} \times \frac{\partial q}{\partial p} = \frac{\theta q}{\theta p} \quad (2.4.1)$$

Where θ_p is the x% perturbation about the parameter of interest, p, and θ_q is the response to the perturbation. Hence, θq = x% × S (p, q) will determine the percentage change of quantity of interest when parameter of interest p changes by x%.

Table 2.4.1 Local Sensitivity Indices S (p, q) with respect to key parameters of interest (each column). Each row are the quantities of interest observed in Figure 2.4.1. Each entry represents a x% change of the QOI with respect to a 10% change in the POI. For instance, a 10% increase in leads to a 1.1% decrease in V yet increases $I*$ and $G*$ by 0.93% and 0.89% respectively.*

	χ	μ	ϵ	γ	r	m	δ	r
V^*	0.038	0.11	-0.14	-0.76	-1.4	0.21	0.23	-0.13
I^*	-0.59	0.67	0.61	-0.67	0.4	0.36	-0.011	-0.2
G^*	-0.17	0.093	0.53	-0.45	0.37	0.35	-0.0068	0.058
R_e	1	0	-0.82	-0.18	0	0	-1e-07	0

2.5 Rich Dynamical Patterns for Coevolution of Pandemic and Infodemic

We observe three predominant patterns for the Co-evolution of Pandemic and Infodemic model. One, at intermediate rate of μ = 0.10 and low values of r = 0.34, the system undergoes displays low frequency high amplitude of vaccination stable oscillations (Figure 2.5.1 **A**, **D**, **G)**. Two, at exceptional low values of r = 0.09 and intermediate μ = 0.10, the system transitions to stable focus of high infection and vaccination corresponding to co-existence in epidemic and vaccination (Figure 2.5.1 **B**, **E**, **H)**. Three, at low values of r = 0.374, and high values of μ = 0.24, the system displays high frequency stable oscillations of low infection (Figure 2.5.2 **C**, **F**, **I).**

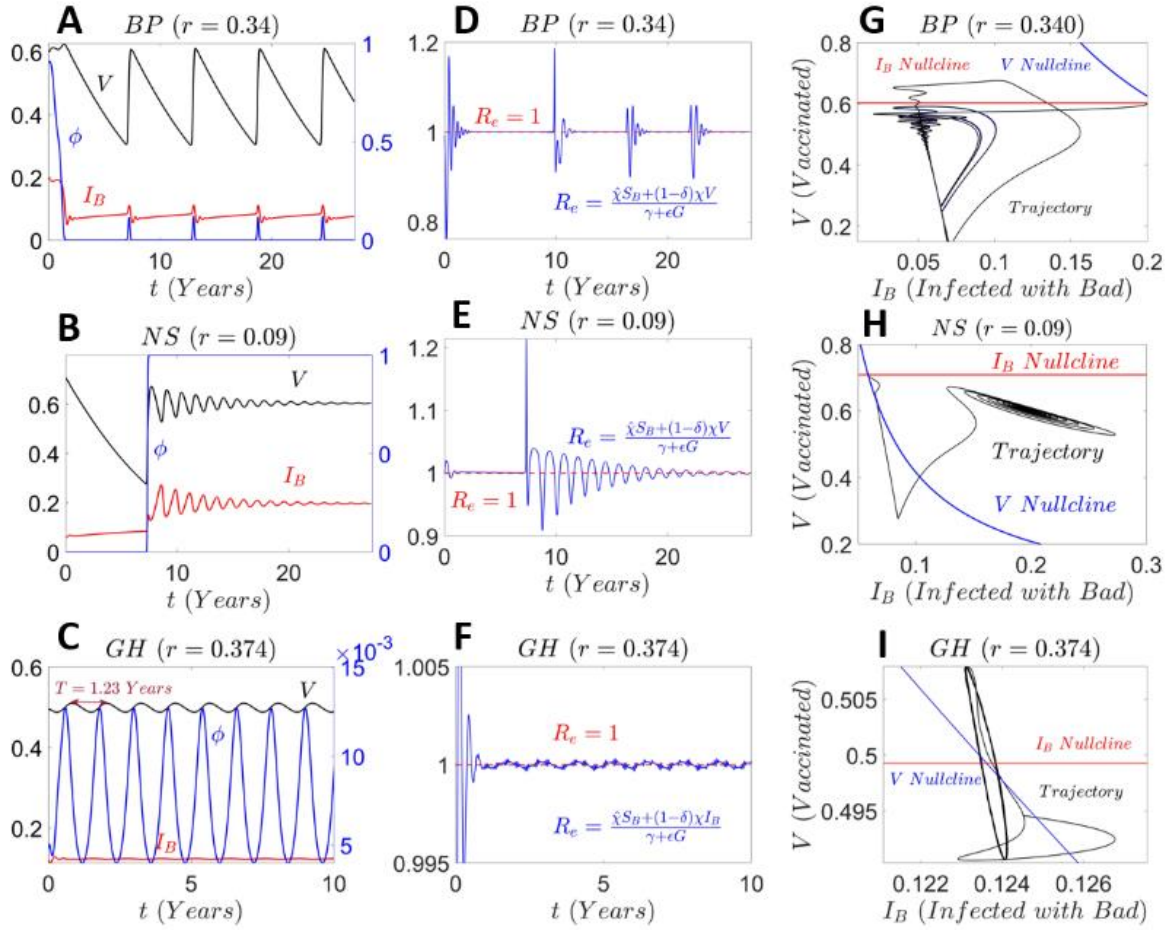

Figure 2.5.1: Three simple dynamics emerge from the co-evolution model. The three columns represent the time evolution of state variables, effective reproductive number, and phase portraits respectively. A, D, G: The system undergoes mixed oscillations of low amplitude low frequency of infection. B, E, H: The system exhibits stable focus of high infection and infection. C, F, I: The system undergoes a stable periodic oscillation of low infection (here μ = 0.24). Initial conditions about the steady states in Figures 2.7.1, 2.7.2 using the algorithm in section 2.2.3.

2.6 Infodemic Drives Pandemic: Stopping Infodemic is necessary to stop Epidemic

To evaluate the spread of bad information in COVID-19, we start along the unstable Hopf with r = 1.635 and vary μ as a bifurcation parameter. We observe that increasing the spread of bad information increases the infection and, not surprisingly, reduces the good information in the population (Figure 2.6.1). We observe the system transitions into stable oscillations of low

infection at lower values of μ, while intermediate values of μ lead to unstable mixed oscillations, and high values of μ drive the system to stable focus of high infection (Figures: 2.6.1, 2.6.2). Notably, at high levels of good information and intermediate values of bad information, the system transitions into high frequency oscillations with low peaks of infection (Figure 2.6.3). Hence, increasing the spread of good information is a sufficient method of public health mitigation policy for reducing the severity of pandemic. It should be noted that our model fails to account for the existence of super spreaders of bad information, which may have strong contribution of infection spread (Section 3, [41]).

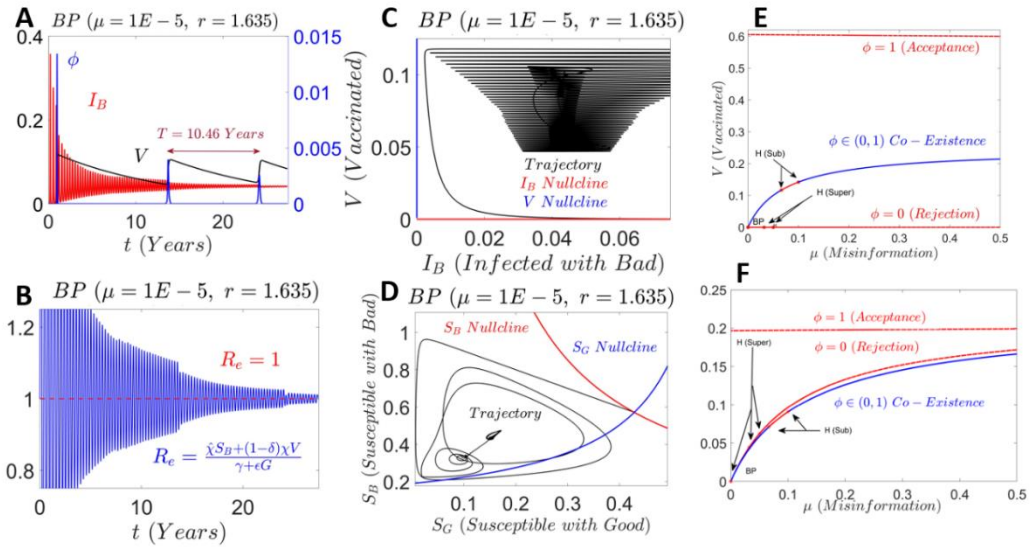

*Figure 2.6.1: **A – B**: Time series evolution of the state variables and effective reproductive number respectively. **C – D**: Phase portraits for the respective time series in column 1. **E – F**: Fixed points with respect to μ. blue and red lines represent stable and unstable fixed points respectively. BP's represent branching point bifurcations where the fixed point has an identical zero eigenvalue. NS's represent neutral saddle equilibrium; a saddle node with an identical zero normal form coefficient. H's represent Andronov-Hopf bifurcations with a pair of purely imaginary eigenvalues. Initial conditions are set about a perturbation of the branching point bifurcation using algorithm 2.2.3. At high r the system displays mixed oscillations and decreasing μ drives the system to DFE.*

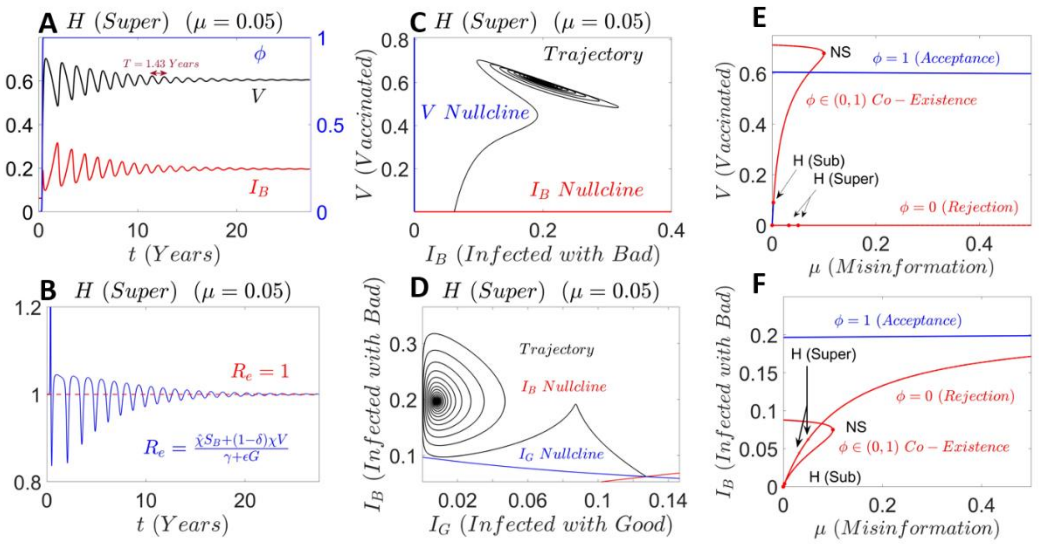

Figure 2.6.2: ***A – B****: Time series evolution of the state variables and effective reproductive number respectively.* ***C – D****: Phase portraits for the respective time series in column 1.* ***E – F****: Fixed points with respect to μ. blue and red lines represent stable and unstable fixed points respectively. NS's represent neutral saddle equilibrium; a saddle node with an identical zero normal form coefficient. H's represent Andronov-Hopf bifurcations with a pair of purely imaginary eigenvalues. Initial conditions are set about a perturbation of the Hopf bifurcation using algorithm 2.2.3. At low r the system is unstable for low values of μ.*

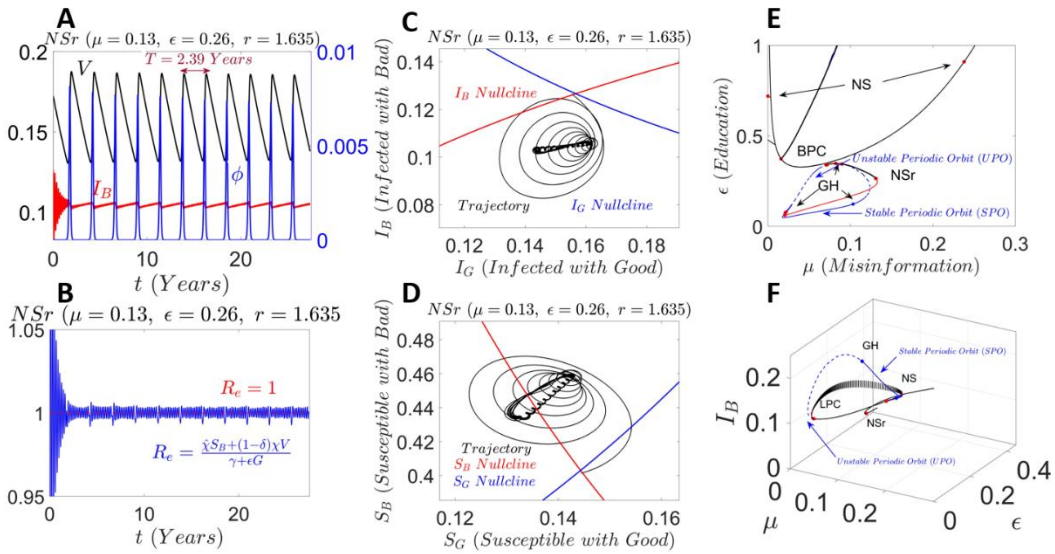

Figure 2.6.3: ***A – B****: Time series evolution of the state variables and effective reproductive number respectively.* ***C – D****: Phase portraits for the respective time series in column 1.* ***E – F****: Fixed points with respect to μ, ϵ. Solid and dotted lines represent stable and unstable periodic orbits respectively. BPC's correspond to branching point of cycles*

corresponding to the intersection between stable focus and unstable periodic orbit. NS's represent neutral saddle equilibrium; a saddle node with an identical zero normal form coefficient. NSr's represent Neimark-Sacker giving birth to a closed invariant curve from a fixed point. H's represent Andronov-Hopf bifurcations with a pair of purely imaginary eigenvalues. Initial conditions are set about a perturbation of the Neimark-Sacker bifurcation using algorithm 2.2.3. The system displays unstable periodic orbits at high values of r and low values of μ.

2.7 High Risk Perception of Infection Promotes Vaccination

One example of high risk is the disproportional perception of vaccine risk and vaccine hesitancy [28]. To determine the effect of vaccine hesitancy and resistance to long term epidemic mitigation, we consider the uptake of vaccination: φ to depend on the relative risk of vaccination to infection. In the context of COVID-19, r corresponds to the risk perception of infection relative to vaccination, although previous models have considered the relative morbidity risk of vaccination relative to infection [6]. Our interpretation of risk perception is due to the controversy regarding rumors associated to the vaccine throughout its development [15, 30]. Mathematically, r corresponds to the dimensionless parameter that determines the probability of vaccination uptake, which is determined using game theory (Sections: 2.2 - 2.4). Asymptotically, the probability of vaccination, φ, converges to zero provided the incentive to vaccinate $\Delta E = I - rV$ is positive leading to the transition into stable focus (Figures: 2.7.1, 2.7.2). When the risk, r, is identically 0, there is always an incentive to vaccinate for any non-zero φ and non-negative I value. Since our theoretical formulation of vaccination follows a coordination game, there exists an unstable mixed Nash Equilibria for non-trivial φ [20] for a critical $r*$ (Sections: 2.2 - 2.4). The critical $r*$ corresponds to the emergence of periodic oscillations and the constant changing of epidemic selection strategy [20]. Furthermore, the branching point bifurcation with and identical zero eigenvalue corresponds to value of $\varphi = 1$ concomitant with the identity: $\Delta E = 0$ (Figure 2.7.1, Section 2.3). We identify at intermediate values of risk; stable periodic oscillations begin

to emerge along the branching point and Hopf bifurcations (Figure 2.7.1). The branching point indicates a point in the domain where no local neighborhood will converge to a point in the local region drifts away towards a region corresponding to the limit cycles [16]. Our results are consistent with survey data that suggest that intermediate values of risk perception of vaccination may hinder the achievement of herd immunity as indicated by the emergence of stable limit cycles and oscillations about Re = 1 (Figures: 2.5.1, 2.5.2) [9, 23, 30]. We observe that decreasing the risk perception of vaccination relative to infection decreases infection and increases vaccination (Figure 2.7.1). Notably, concomitant decrease in the spread of corona-misinformation along with reduction of risk perception of vaccination is sufficient to drive the system to DFE. At low risk and high spread of bad information, the system transitions to stable focus of high infection (Figure 2.7.2). These results may be understood from a game theoretical perspective by analyzing the risk function (equation 2.1.6, Section 2.3). The intersection of the stable focus boundary (in red) and limit cycle continuation (in blue) corresponds to the emergence of the branching point bifurcation (BP), which phenomenologically separates the stable focus of infection from the persistent low frequency stable oscillations (Figures: 2.7.1, 2.7.2). One observes that risk, $r = r_v/r_i$, is the risk perception of vaccination relative to infection, it follows that decreasing the relative risk is equivalent to increasing the risk of infection relative to vaccination. Thus, this implies that high risk perception of infection leads to an increase in vaccination. In other words, when the population takes the virus seriously, there is decreased epidemiological severity. Additionally, intermediate risk leads to high frequency infection and supports the notion that vaccination hesitancy promotes the propagation of disease [15, 31].

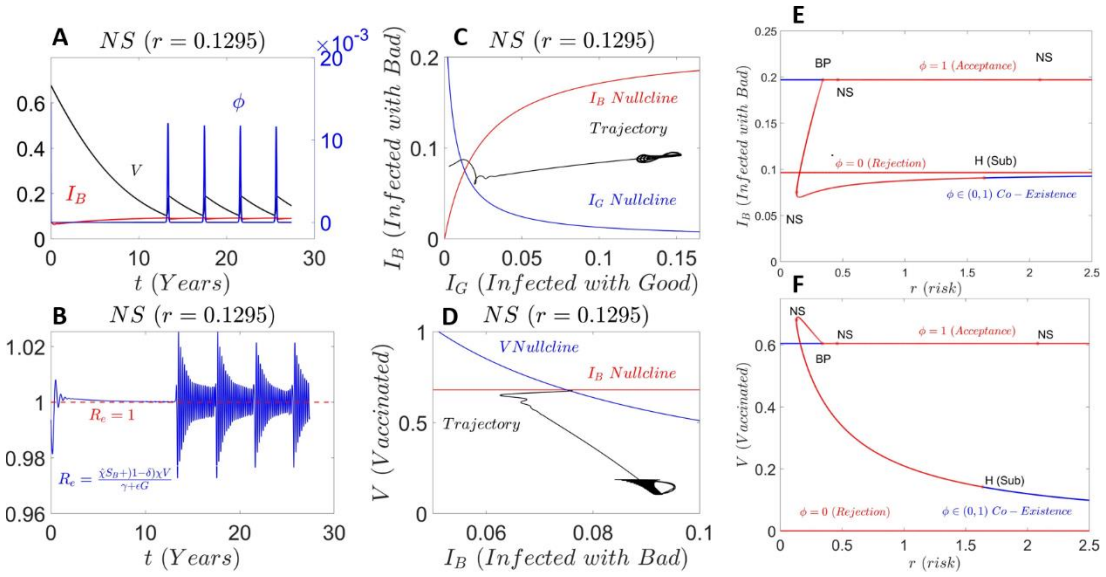

Figure 2.7.1: ***A – B****: Time series evolution of the state variables and effective reproductive number respectively.* ***C – D****: Phase portraits for the respective time series in column 1.* ***E – F****: Fixed points with respect to r. blue and red lines represent stable and unstable fixed points respectively. BP's represent branching point bifurcations where the fixed point has an identical zero eigenvalue. NS's represent neutral saddle equilibrium; a saddle node with an identical zero normal form coefficient. H's represent Andronov-Hopf bifurcations with a pair of purely imaginary eigenvalues. Initial conditions are set about a perturbation of the neutral saddle bifurcation using algorithm 2.2.3.*

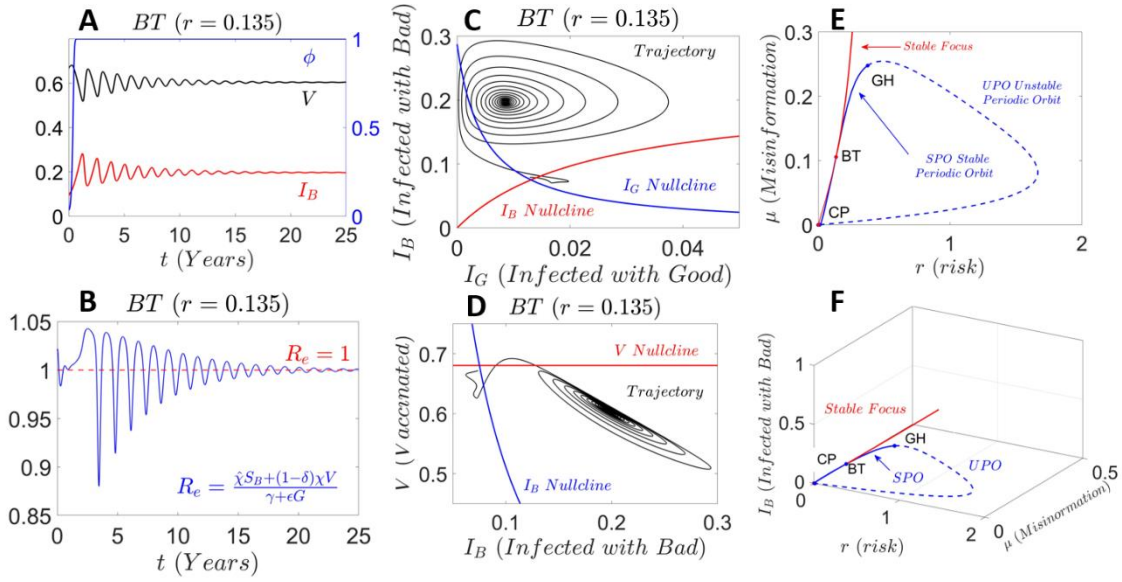

Figure 2.7.2: ***A – B****: Time series evolution of the state variables and effective reproductive number respectively.* ***C – D****: Phase portraits for the respective time series in column 1.* ***E – F****:*

Fixed points with respect to r, μ. Solid and dotted lines represent stable and unstable periodic orbits respectively. Blue and red curves correspond to periodic orbit and stable focus boundaries respectively. CP's represent cusp bifurcations corresponding to a saddle node bifurcation with zero normal form coefficient. NS's represent neutral saddle equilibrium; a saddle node with an identical zero normal form coefficient. BT's represent Bogdanov-Takens correspond to a fixed point with zero eigenvalue with multiplicity two. GH's represent generalized Hopf bifurcations corresponding to the intersection between stable and unstable periodic orbit. Initial conditions are set about a perturbation of the Bogdanov-Takens bifurcation using algorithm 2.2.3. The system displays unstable periodic orbits at high values of r and low values of μ.

2.8 High Vaccination Efficacy Impedes Infection

Previous studies have suggested that willingness to vaccinate is highly coordinated with public perception of risk associated to vaccination [9, 19, 35, 36]. That is, high risk perception of vaccination decreases the likelihood of the population taking the vaccine and impedes the achievement of herd immunity. Since intermediate values of risk play a significant barrier to the achievement of herd immunity [30], we choose to evaluate the role of vaccination efficacy along the unstable branch at the emergence of the sub-critical Andronov-Hopf bifurcation at r = 1.6353 in Figure 2.7.1. We observe that larger vaccine efficacies only reduce the severity (amplitude of infection) and is limited in reducing the endemic state of the endemic (Figure 2.8.1). This is a limitation of the model, which considers the emergence of breakthrough infection, i.e., vaccination leakage, phenomenologically corresponding to the emergence of new strands of COVID-19 in the long run (Section 3).

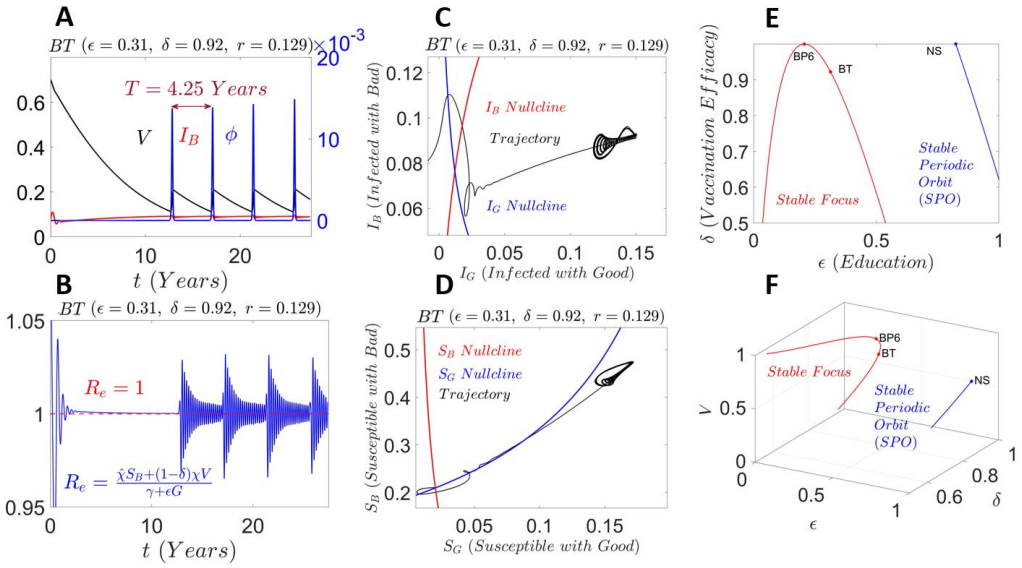

Figure 2.8.1: ***A – B****: Time series evolution of the state variables and effective reproductive number respectively.* ***C – D****: Phase portraits for the respective time series in column 1.* ***E – F****: Fixed points with respect to r, μ. Blue and red curves correspond to periodic orbit and stable focus boundaries respectively. NS's represent neutral saddle equilibrium; a saddle node with an identical zero normal form coefficient. BT's represent Bogdanov-Takens correspond to a fixed point with zero eigenvalue with multiplicity two. BP6's represents branching point bifurcations. Initial conditions are set about a perturbation of the Bogdanov-Takens bifurcation using algorithm 2.2.3. The system displays unstable periodic orbits at high values of r and low values of μ.*

2.9 Education Reduces Infection

Some studies suggest that the spread of misinformation precedes the infection [17], we consider the case where people change their behavior in response to infection. For μ ∈ (0.06, 0.1), we observe mixed oscillations along the unstable branch (Figures: 2.6.1, 2.6.2, 2.6.3). To observe how the promotion of good information, which corresponds to the increase in the rate at which people change behavior in response to infection, we start from the sub-critical Andronov-Hopf bifurcation at μ = 0.10 and vary the rate of education ϵ. We observe that increasing the good information decreases the amplitude of infection yet, increases the mean frequency of infection suggesting that reducing the spread of coronoa-misinformation is necessary to reduce

the onset of limit cycles and stop the infection (Figure 2.6.3). We observe that promoting the education promotes the vaccination and decreases infection, which is obtained for high risk and low risk respectively (Figures: 2.9.1, 2.9.2). Depending on the risk, intermediate education leads to high frequency stable oscillations (Figure 2.9.1) or complex oscillations emerging from an unstable branching point (Figure 2.9.2). The effects of the transmission of good information can be understood by observing Figure 2.9.3; where high risk corresponds to unstable oscillations and low risk corresponds to stable periodic oscillation. From a public health perspective, decreasing the risk perception of the vaccination while promoting education drives the system to disease free equilibrium (Figure 2.9.3: **A**, **C**).

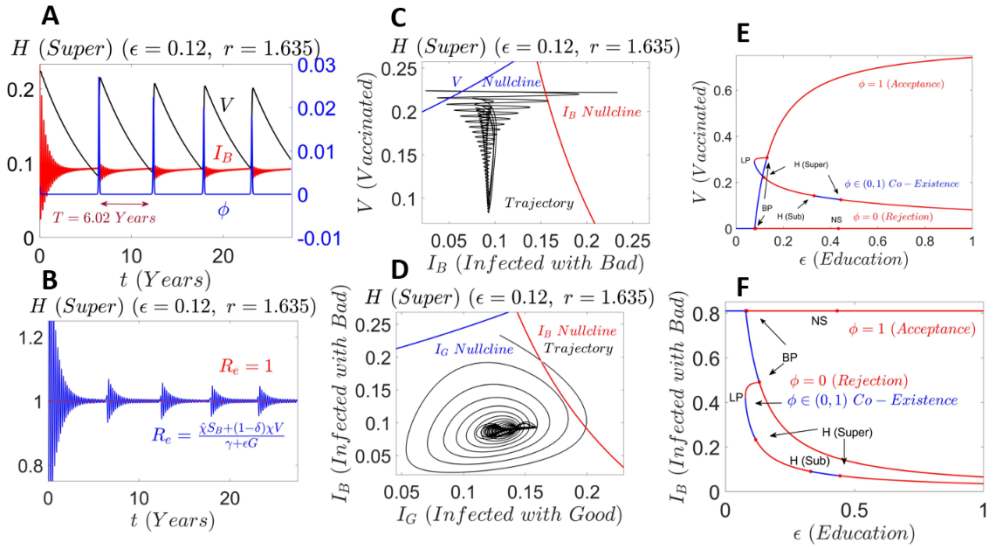

Figure 2.9.1: Time series evolution of the state variables and effective reproductive number respectively. ***C – D****: Phase portraits for the respective time series in column 1.* ***E – F****: Fixed points with respect to ϵ. The blue and red lines represent stable and unstable fixed points respectively. BP's represent branching point bifurcations where the fixed point has an identical zero eigenvalue. NS's represent neutral saddle equilibrium; a saddle node with an identical zero normal form coefficient. H's represent Andronov-Hopf bifurcations with a pair of purely imaginary eigenvalues. LP's represents limit point bifurcations where the fixed point has an identical zero eigenvalue. Initial conditions are set about a perturbation of the Andronov-Hopf bifurcation using algorithm 2.2.3.*

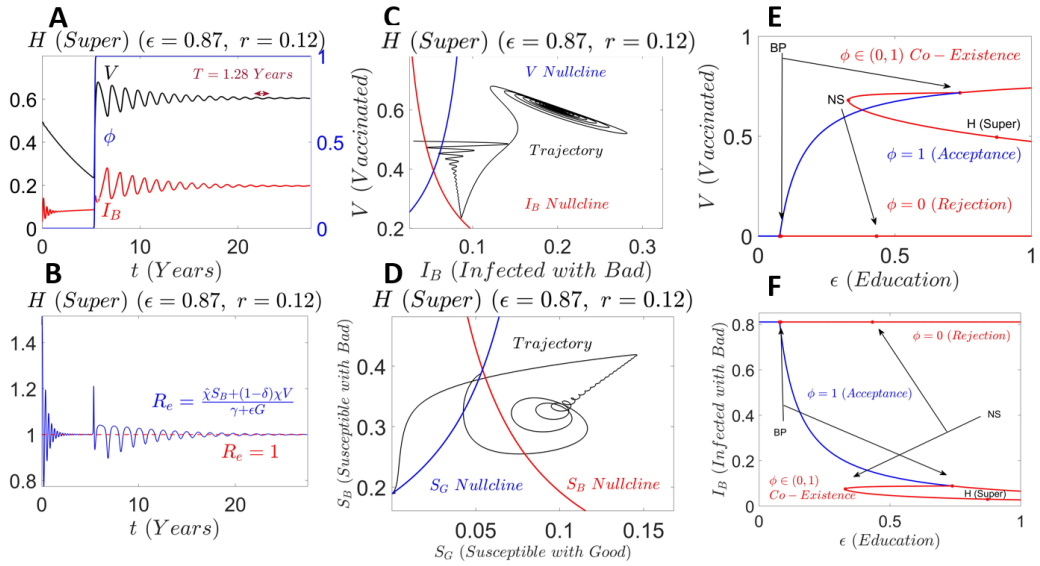

Figure 2.9.2: ***A – B****: Time series evolution of the state variables and effective reproductive number respectively.* ***C – D****: Phase portraits for the respective time series in column 1.* ***E – F****: Fixed points with respect to ϵ. blue and red lines represent stable and unstable fixed points respectively. BP's represent branching point bifurcations where the fixed point has an identical zero eigenvalue. NS's represent neutral saddle equilibrium; a saddle node with an identical zero normal form coefficient. H's represent Andronov-Hopf bifurcations with a pair of purely imaginary eigenvalues. Initial conditions are set about a perturbation of the Andronov-Hopf bifurcation using algorithm 2.2.3.*

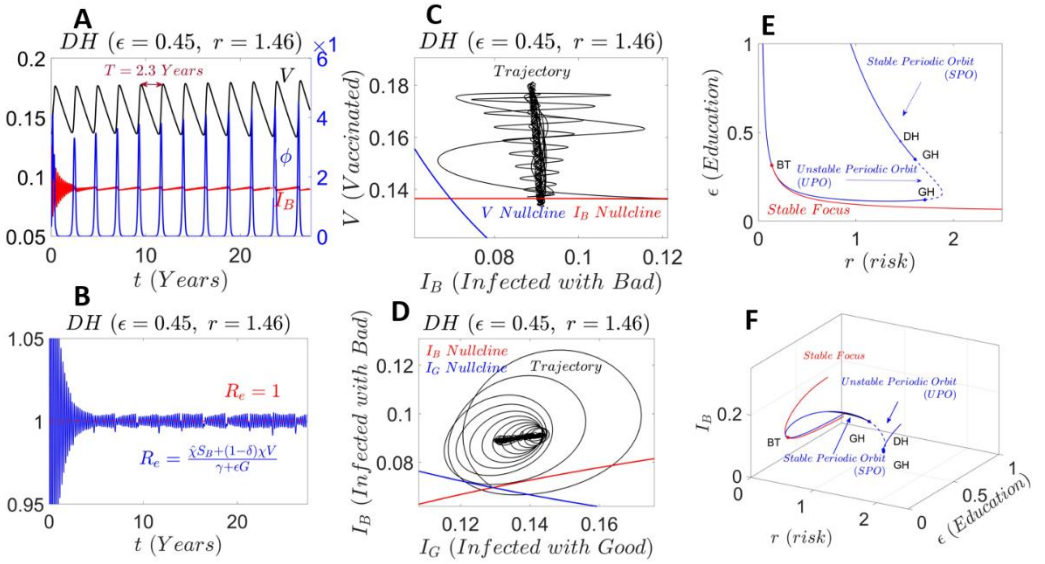

Figure 2.9.3: ***A – B****: Time series evolution of the state variables and effective reproductive number respectively.* ***C – D****: Phase portraits for the respective time series in column 1.* ***E – F****: Fixed points with respect to r, ϵ. Blue and red curves correspond to periodic orbit and stable focus boundaries respectively. DH's represent Double Hopf bifurcations corresponding to two*

distinct pairs of purely imaginary eigenvalues. GH's represent Generalized Hopf bifurcations corresponding to the transition between stable and unstable periodic orbit. BT's represent Bogdanov-Takens correspond to a fixed point with zero eigenvalue with multiplicity two. Initial conditions are set about a perturbation of the Double Hopf bifurcation using algorithm 2.2.3. The system displays unstable periodic orbits for a narrow region of high r.

3 CONCLUSIONS

The COVID-19 pandemic has placed an unprecedented tax on the public economy and health on nations worldwide. This global pandemic is unique as it is the first pandemic to occur in the digital age. The overabundance of bad information related to the coronavirus and vaccine has been recognized as a major hurdle in the combat against the pandemic, acting as a brake on intervention strategies in reducing the spread of infection [3, 41, 42]. An increasing amount of evidence have shown that Covid-19 vaccines not only protect against severe symptoms and deaths due to infection, but are effective in reducing overall infection [8, 10, 34], even against the more infectious Delta variant. One major barrier to the increase in vaccine uptake proponents of public health mitigation is vaccine hesitancy [28, 31]. As a new wave of COVID-19 caused by the Delta variant races across the world, mentions of some phrases prone to vaccine misinformation in July jumped as much as five times the June rate, according to Zignal Labs, which tracks mentions on social media, on cable television and in print and online outlets. Some of the most prevalent falsehoods are that vaccines don't work (up 437 percent), that they contain microchips (up 156 percent), that people should rely on their "natural immunity" instead of getting vaccinated (up 111 percent) and that the vaccines cause miscarriages (up 75 percent)." New York Times reported on August 10, 2021 [1]. To combat the controversial issues regarding COVID-19 vaccination and achievement of herd immunity, we evaluate the concomitant spread of infection and information in the context of emergence of new strands by including a vaccination leakage compartment. At the beginning stages of a pandemic, the infection begins to

take off and people do not take the appropriate precautionary measures to reduce the infection. Since the spread of corona-misinformation precedes the onset of infection, we model the disease infection driven by those carrying bad information [17]. We choose to evaluate the role of vaccination in reducing the spread of infection driven by those with bad information. Since public trust and perception of vaccination significantly contribute to the likelihood of vaccination uptake, we consider modeling the adoption of vaccination, which depends on risk perception of vaccination relative to infection [19, 35]. Using an evolutionary game theoretical framework to model the probability of vaccination uptake, we observe that high perception of risk leads to the emergence of stable limit cycles corresponding to a persistent state of infection (Figures: 2.7.1, 2.7.2). Lastly, we observe that although good information reduces the severity of infection, reduction in the spread of bad information is sufficient to inhibit the recurrence and severity of infection (Figures: 2.6.1, 2.6.2, 2.6.3). Since our model considers the spread of corona-misinformation to require physical interaction between good and bad information domains, reducing the spread of bad information delays the recurrence of infection is obtained by limiting the interaction between good and bad information domains and not by reducing the abundance of information. Additionally, our model fails to discriminate between disinformation and misinformation, the key difference focusing on the malicious intent of the latter.

Furthermore, we note that our model considers the spread of information which requires physical contact between good and bad domain carriers and is independent of the quantity of information exchange [41]. We consider the probability of vaccination uptake, which is derived using classical evolutionary game theory replicator equations [20]. Lastly, we consider an SIS model with temporary immunity of vaccination due to the potential for the emergence of new COVID-19 variants, which act as a brake on the achievement of herd immunity and supports the

recurrence of future infection [5]. We note that other frameworks that model the impact of information on infection consider SEIR type disease domain models [39, 41]. Since the vaccination compartment has a leakage and the vaccinated become re-infected, then the achievement of herd immunity cannot be obtained by increasing the fraction of the population to become vaccinated. Hence, vaccination only acts as a temporal delay on the infection spread rather than decrease on long term epidemiological severity. This differs from mathematical models that considers vaccinated individuals to return to the susceptible compartment [6].

3.1 Future Directions

Alternative approaches to our model may consider using a SEIR with a vaccination compartment focused on a specific strand or an SIR model in the disease domain. Our model is catered to the potential emergence of new strands of COVID-19 in the long run. We may also alter the risk function to include information in the payoff calculation Our results suggest that even at vaccination efficacy as high as 90%, reducing the spread of bad information is necessary to stop the spread of infection; supporting public health mitigation strategies that focus on information exchange. Additionally, our model is limited in a compartmental framework, which assumes equal probability of transmission throughout the population. The compartmental model is not the most representative spread of information, since most digital and social networks admit super spreaders with higher levels of spread. Our model may be extrapolated onto a bipartite network in which the information domain takes the form of a social network, and the disease domain takes the form of scale free network. Alternatively, one may consider modeling the transmission between stratified aged populations in the disease domain. It would be interesting to see how the results depend on the connectivity of the hubs. Like Ye's framework, one may consider the bipartite network in lieu of the stratified SIS model [41]. Although the results of the

co-evolution of pandemic and infodemic are limited to the context of emerging strands of COVID-19, the modelling of information exchange may be extrapolated to the exchanging of ideas. The exchanging of ideas requires close communication between sender and receiver and this interaction may be assumed to be non-linear since the absence of sender or receiver may lead to a lack of idea exchange. As thoughts, which are often driven by information received and interpreted, and actions are driven by initiative. The stable oscillations in the co-evolution model may be interpreted as robust interplay between thoughts and actions.

REFERENCES

[1] Davey Alba. Virus misinformation spikes as delta cases surge, 2021.

[2] Oberiri Destiny Apuke and Bahiyah Omar. Fake news and COVID-19: modelling the predictors of fake news sharing among social media users. Telematics and Informatics, 56:101475–101475, 2021.

[3] Oberiri Destiny Apuke and Bahiyah Omar. Fake news and covid-19: modelling the predictors of fake news sharing among social media users. Telematics and Informatics, 56:101475, 2021.

[4] Leon Arriola and James M Hyman. Sensitivity analysis for uncertainty quantification in mathematical models. In Mathematical and statistical estimation approaches in epidemiology, pages 195–247. Springer, 2009.

[5] C. Aschwanden. Five reasons why covid herd immunity is probably impossible. Nature, 591(7851):520–522, 2021.

[6] Chris T. Bauch and David J. D. Earn. Vaccination and the theory of games. Proceedings of the National Academy of Sciences of the United States of America, 101(36):13391, 2004.

[7] Julii Brainard and Paul Hunter. Misinformation making a disease outbreak worse: outcomes compared for influenza, monkeypox, and norovirus. SIMULATION, 96:003754971988502, 11 2019.

[8] CM Brown, J Vostok, and H et al. Johnson. Outbreak of sars-cov-2 infections, including covid-19 vaccine breakthrough infections, associated with large public gatherings — barnstable county, massachusetts, july 2021. MMWR Morb Mortal Wkly Rep, 70:1059–1062, 2021.

[9] Marta Caserotti, Paolo Girardi, Enrico Rubaltelli, Alessandra Tasso, Lorella Lotto, and Teresa Gavaruzzi. Associations of COVID-19 risk perception with vaccine hesitancy over time for italian residents. Social Science& Medicine, 272:113688, 2021.

[10] AM Cavanaugh, KB Spicer, D Thoroughman, C Glick, and K Winter. Reduced risk of reinfection with sars-cov-2 after covid-19 vaccination — kentucky, may–june 2021. MMWR Morb Mortal Wkly Rep, 70:1081–1083, 2021.

[11] RH Clewley, WE Sherwood, MD LaMar, and JM Guckenheimer. Pydstool, a software environment for dynamical systems modeling, 2007. 21

[12] Angelo Coluccia. On the probabilistic modeling of fake news (hoax) persistency in online social networks and the role of debunking and fitering. Internet Technology Letters, 3, 07 2020.

[13] Jessica R Conrad, Ling Xue, Jeremy Dewar, and James M Hyman. Modeling the impact of behavior change on the spread of ebola. In Mathematical and Statistical Modeling for Emerging and Re-emerging Infectious Diseases, pages 5–23. Springer, 2016.

[14] Odo Diekmann, Johan Andre Peter Heesterbeek, and Johan AJ Metz. On the definition and the computation of the basic reproduction ratio R0 in models for infectious diseases in heterogeneous populations. Journal of mathematical biology, 28(4):365–382, 1990.

[15] Amiel A. Dror, Netanel Eisenbach, Shahar Taiber, Nicole G. Morozov, Matti Mizrachi, Asaf Zigron, Samer Srouji, and Eyal Sela. Vaccine hesitancy: the next challenge in the fight against covid-19. European Journal of Epidemiology, 35(8):775–779, 2020.

[16] P. Fitzpatrick and Jacobo Pejsachowicz. Branching and bifurcation. Discrete& Continuous Dynamical Systems - S, 12:1955–1975, 01 2018.

[17] Riccardo Gallotti, Francesco Valle, Nicola Castaldo, Pierluigi Sacco, and Manlio De Domenico. Assessing the risks of ‘infodemics’ in response to COVID-19 epidemics. Nature Human Behaviour, 4(12):1285–1293, 2020.

[18] Josef Hofbauer and Karl Sigmund. Evolutionary game dynamics. Bulletin of the American Mathematical Society, 40(4):479–519, 2003.

[19] Seonghoon Hong and Alan Collins. Societal responses to familiar versus unfamiliar risk: Comparisons of influenza and sars in korea. Risk Analysis, 26(5):1247–1257, 2006.

[20] S. Hummert, K. Bohl, D. Basanta, A. Deutsch, S. Werner, G. Theissen, A. Schroeter, and S. Schuster. Evolutionary game theory: cells as players. Mol Biosyst, 10(12):3044–65, 2014.

[21] K. M. A. Kabir and J. Tanimoto. Evolutionary game theory modelling to represent the behavioural dynamics of economic shutdowns and shield immunity in the COVID-19 pandemic. R Soc Open Sci, 7(9):201095, 2020.

[22] Kin On Kwok, Kin-Kit Li, Wan In Wei, Arthur Tang, Samuel Yeung Shan Wong, and Shui Shan Lee. Editor's choice: Influenza vaccine uptake, covid-19 vaccination intention and vaccine hesitancy among nurses: A survey. International journal of nursing studies, 114:103854–103854, 2021.

[23] Pedro Almeida Laires, S´onia Dias, Ana Gama, Marta Moniz, Ana R Pedro, Patricia Soares, Pedro Aguiar, and Carla Nunes. The association between chronic disease and serious COVID-19 outcomes and its influence on risk perception: Survey study and database analysis. JMIR Public Health Surveill, 7(1):e22794, Jan 2021.

[24] Jeffrey V. Lazarus, Scott C. Ratzan, Adam Palayew, Lawrence O. Gostin, Heidi J. Larson, Kenneth Rabin, Spencer Kimball, and Ayman El-Mohandes. A global survey of potential acceptance of a COVID-19 vaccine. Nature Medicine, 27(2):225–228, 2021. 22

[25] Richard P. Mann. Collective decision making by rational individuals. Proceedings of the National Academy of Sciences, 115(44):E10387, 2018.

[26] J. McAteer, I. Yildirim, and A. Chahroudi. The vaccines act: Deciphering vaccine hesitancy in the time of covid-19. Clin Infect Dis, 71(15):703–705, 2020.

[27] T. Murayama, S. Wakamiya, E. Aramaki, and R. Kobayashi. Modeling the spread of fake news on twitter. PLoS One, 16(4):e0250419, 2021.

[28] Jamie Murphy, Fr´ed´erique Valli`eres, Richard P. Bentall, Mark Shevlin, Orla McBride, Todd K. Hartman, Ryan McKay, Kate Bennett, Liam Mason, Jilly Gibson-Miller, Liat Levita, Anton P. Martinez, Thomas V. A. Stocks, Thanos Karatzias, and Philip Hyland. Psychological characteristics associated with covid-19 vaccine hesitancy and resistance in ireland and the united kingdom. Nature Communications, 12(1):29, 2021.

[29] Christopher J. L. Murray and Peter Piot. The potential future of the COVID-19 pandemic: Will sars-cov-2 become a recurrent seasonal infection? JAMA, 325(13):1249–1250, 2021.

[30] Elise Paul, Andrew Steptoe, and Daisy Fancourt. Attitudes towards vaccines and intention to vaccinate against COVID-19: Implications for public health communications. The Lancet Regional Health - Europe, 1, 2021.

[31] M. S. Razai, T. Osama, D. G. J. McKechnie, and A. Majeed. Covid-19 vaccine hesitancy among ethnic minority groups. Bmj, 372:n513, 2021.

[32] Daniel Romer and Kathleen Hall Jamieson. Conspiracy theories as barriers to controlling the spread of covid-19 in the u.s. Social Science & Medicine, 263:113356, 2020.

[33] Jon Roozenbeek, Claudia R. Schneider, Sarah Dryhurst, John Kerr, Alexandra L. J. Freeman, Gabriel Recchia, Anne Marthe van der Bles, and Sander van der Linden. Susceptibility to misinformation about covid-19 around the world. Royal Society Open Science, 7(10):201199, 2020.

[34] ES Rosenberg, DR Holtgrave, V Dorabawila, M Conroy, D Greene, E Lutterloh, B Backenson, D Hoefer, J Morne, U Bauer, and HA Zucker. New covid-19 cases and

hospitalizations among adults, by vaccination status — new york, may 3–july 25, 2021. MMWR Morb Mortal Wkly Rep, 70:xxxx–xxxx, 2021.

[35] Philipp Schmid, Dorothee Rauber, Cornelia Betsch, Gianni Lidolt, and Marie-Luisa Denker. Barriers of influenza vaccination intention and behavior–a systematic review of influenza vaccine hesitancy, 2005–2016. PloS one, 12(1):e0170550, 2017.

[36] Michel Setbon and Jocelyn Raude. Factors in vaccination intention against the pandemic influenza A/H1N1. European Journal of Public Health, 20(5):490–494, 05 2010.

[37] Viroj Tangcharoensathien, Neville Calleja, Tim Nguyen, Tina Purnat, Marcelo D'Agostino, Sebastian Garcia-Saiso, Mark Landry, Arash Rashidian, Clayton Hamilton, Abdelhalim AbdAllah, Ioana Ghiga, Alexandra Hill, Daniel Hougendobler, Judith van Andel, Mark Nunn, Ian Brooks, Pier Luigi Sacco, Manlio De Domenico, Philip Mai, Anatoliy Gruzd, Alexandre Alaphilippe, 23 and Sylvie Briand. Framework for managing the covid-19 infodemic: Methods and results of an online, crowdsourced who technical consultation. J Med Internet Res, 22(6):e19659, Jun 2020.

[38] Thomas L. Vincent and Joel S. Brown. Stability in an evolutionary game. Theoretical Population Biology, 26(3):408 – 427, 1984.

[39] Yi Wang, Jinde Cao, Zhen Jin, Haifeng Zhang, and Gui-Quan Sun. Impact of media coverage on epidemic spreading in complex networks. Physica A, 392(23):5824–5835, 2013.

[40] WHO. Managing the covid-19 infodemic: Promoting healthy behaviours and mitigating the harm from misinformation and disinformation, 09 2020.

[41] Mengbin Ye, Lorenzo Zino, Alessandro Rizzo, and Ming Cao. Modelling collective decisionmaking during epidemics, 2020.

[42] Zilong Zhao, Jichang Zhao, Yukie Sano, Orr Levy, Hideki Takayasu, Misako Takayasu, Daqing Li, Junjie Wu, and Shlomo Havlin. Fake news propagates differently from real news even at early stages of spreading. EPJ Data Science, 9(1):7, 2020